Proceedings of the IASS Annual Symposium 2025
"The living past as a source of innovation"
October 27 – 31, 2025, México City, México
Juan Gerardo Oliva, Juan Ignacio del Cueto, Elisa Drago Quaglia (eds.)

Design of Concrete 3D Printed, Post-Tensioned Spanning Structures with Embedded Triply Periodic Minimal Surfaces

Maximilian E. ORORBIA[*,a], Amir MOTAVASELIAN[a], Hua CHAI[a], Ryan WELCH[b], Masoud AKBARZADEH[a]

[a] Polyhedral Structures Laboratory, Weitzman School of Design, University of Pennsylvania
Pennovation Center, 3401 Grays Ferry Ave. Philadelphia, PA, 19146, USA
[*]mororbia@upenn.edu

[b] KieranTimberlake, Philadelphia, US

Abstract

Periodic anticlastic surfaces can perform well for concrete structural applications due to their efficient distribution of stress under compression and are possible for large scale construction through advanced manufacturing technologies. Spanning structures designed using anticlastic surfaces, specifically diamond triply periodic minimal surfaces, can reduce concrete volume while meeting performance metrics set by design codes without requiring significant steel reinforcement. This work presents a design approach that generates and assesses spanning concrete, post-tensioned structures with embedded periodic anticlastic surfaces. Each generated design is evaluated based on its flexural strength, applied post-tensioning forces, concrete and steel quantities, and environmental impacts. The design and assessment approach developed here is applied to a pedestrian bridge example ensuring that each design's flexural strength (nominal moment capacity) exceeds the bending moment caused by self-weight and applied live loading as well as minimizing mass and emitted carbon dioxide. In comparison to a set of incumbent structures, the generated periodic anticlastic designs achieve desired performance while reducing overall materials as well as environmental impacts, achievable through the realization of complex geometries with advanced construction technologies.

Keywords: Design generation and assessment, embedded triply periodic minimal surfaces, carbon emissions, concrete 3D-printing, post-tensioning

1. Introduction

A comprehensive computational design approach, including form-finding, volumetric modeling, and digital fabrication, was developed for a prefabricated, funicular concrete beam, DIAMANTI, recently exhibited at the European Cultural Centre's 2025 biennial exhibition [1, 2]. Through the beam's design, fabrication, construction, and testing [3] (see Fig. 1), DIAMANTI demonstrated that 3D-printed concrete, post-tensioned modular spanning structures can exceed flexural strength design standards as well as achieve serviceability and resiliency. This type of structure and construction can be an economical alternative through its reduction of materials, for example, reducing concrete and steel as well as eliminating the need for formwork. In this work, the design approach [1, 3, 4, 5, 6] is extended to generate and assess structures for larger spans.

Polyhedral graphic statics (PGS), a geometry-based design framework ensuring equilibrium through the reciprocal relationship between geometric form and forces, allows designers to visualize and control the flow of forces across complex geometries [7, 6]. In prior work [1], unit cells derived from PGS provided

Figure 1: Constructed 5-meter funicular concrete beam, DIAMANTI, with embedded anticlastic surfaces. Also constructed at 10 meters, DIAMANTI underwent flexural strength testing, demonstrating how concrete 3D-printed, post-tensioned modular structures can offer an economical, less wasteful, and lighter solution compared to conventional construction [3].

a flexible, modular approach in generating light-weight beam structures with embedded diamond triply periodic minimal surface (TPMS) geometries. Advanced construction technologies, including concrete 3D-printing, allowed for the physical realization of the complex TPMS geometries and post-tensioning, compressing the modular segments together, further enhanced structural performance [3]. Altogether the workflow achieved a sustainable beam design (at 3, 5, and 10 meters in length) by reducing construction material usage without compromising structural integrity, offering a strategy to generate light weight, high performing concrete structures for architectural and civil engineering applications.

Here, the use of the PGS-TPMS workflow is further developed to generate structures with larger spans, ideal for pedestrian bridge designs where achieving structural efficiency, material economy, and aesthetic elegance are typical objectives. As such, the developed method generates and approximately assesses multiple design alternatives. In particular, the flexural strength of the TPMS structures is assessed and the amount of post-tensioning cables and required jacking force needed to meet strength and offset specified loading is evaluated. This work establishes a basis for early conceptual design space exploration of such concrete 3D-printed and post-tensioned TPMS spanning structures.

The paper is organized as follows: Section 2 provides an overview of generating designs with embedded TPMS and assessing their flexural strength and post-tensioning requirements. In Section 3, six pedestrian bridge designs are generated and compared to incumbent spanning structures. All designs are assessed by their flexural strength as well as the amount of materials needed, including concrete and post-tensioning reinforcement, contextualized by their environmental impact of carbon emissions. Closing remarks are made in Section 4, discussing the promise of such designs resulting in lighter and economical structures that have improved performance, serviceability and resiliency.

2. Spanning TPMS Structural Generation and Assessment

The following section discusses how triply periodic minimal diamond geometries are embedded in unit cells derived from polyhedral graphic statics. Due to the complex geometry generated for the structure, an approximate analysis of the nominal moment capacity and required amount of post-tensioning cables

and applied jacking, tensioning force is developed. Capable of generating and assessing design alternatives, a design goal, objective as well as variables and constraints are set to guide the design process in generating desired solutions.

2.1. Structural Form-Finding and TPMS Embedding

Using PGS [7, 6] as a form-finding approach, unit cells are derived and populated with TPMS through volumetric modeling. Rather than materializing individual edges or faces, PGS-derived volumetric cells are treated as spatial hulls, force-informed boundaries, within which TPMS geometries are embedded. This process is illustrated in Fig. 2. Initially, separate from the PGS unit cells, a diamond TPMS geometry, parametrically defined with a wavelength set to one, is bound within a set box. Scale transformations are made to better populate the box with the TPMS geometry and further control preliminary porosity. After centering and applying other operations, cutting and mirroring, to achieve symmetry, the TPMS geometry is morphed via twisted box transformations to conform to the PGS unit cell while preserving the minimal surface characteristics essential for uniform force distribution and high stiffness-to-weight

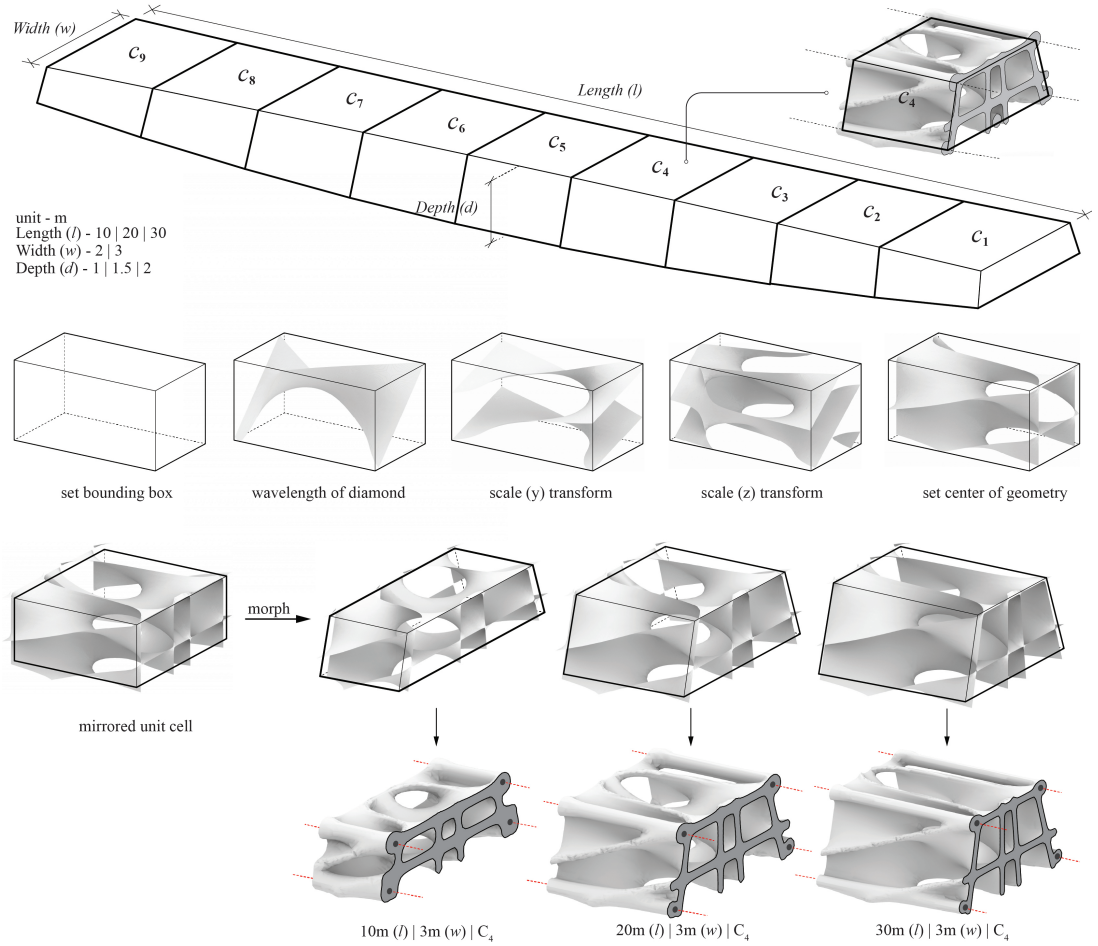

Figure 2: Structural form-finding through polyhedral graphic statics and volumetric modelling with periodic anticlastic surfaces and volume generation. Diamond TPMS are geometrically manipulated and transformed to conform within PGS unit cells. Mesh thickened surfaces are adapted to incorporate post- tensioning conduits. Here, this approach is applied to three different unit cells derived from PGS forms with different spans showcasing geometric differences, including the concrete-cross sections.

ratios. The resulting thickened mesh is converted into a distance field to enable precise surface offsetting for extrusion-based concrete 3D-printing. Additional functional adaptations are applied, including post-tensioning cable conduits, by aligning key features of the TPMS geometry with primary force paths and modulating cross-sectional geometry accordingly.

2.2. Approximate Strength and Post-Tensioning Assessment

An approximate analysis was developed to calculate the flexural strength of the TPMS spanning structure since its embedded geometry has varying cross-section along its length, considering the structure as non-prismatic. Assuming simple supports, restraining the horizontal R_x and vertical R_y degrees of freedom (D.o.F.) at one end and the vertical D.o.F. at the other, the nominal moment capacity, M_n, is calculated at mid-span where the bending moment caused by the applied loading is at its maximum, M_u. For the analysis considered here, the applied load is determined by the distributed live load across the top surface of the beam and the self-weight of the structure. Material properties and the cross-section geometry influence the TPMS structure's nominal moment capacity. For the prefabricated, post-tensioned TPMS concrete structure, the following formula was applied:

$$M_n = A_{PT} f_{py} (d - \frac{0.85a}{2}) \tag{1}$$

where A_{PT} is the area of steel determined from the post-tensioned cable, f_{py} is the yield strength of the cable, d is the effective depth locating the cable within the cross-section, and a is the depth of the simplified concrete compressive stress block (Fig. 3). The compressive depth is determined based on the equilibrium of forces at ultimate load in which the internally developed tensile and compressive forces within the concrete structure are balanced. For standard designed prismatic-concrete structures, with constant cross section over their length, the compressive force is determined by equating the compressive force to 85% of the concrete's ultimate strength, f'_c, multiplied by the concrete area in compression. Similarly, the tensile force is determined by multiplying the total area of steel in tension by the steel's yield strength, f_y. By equating the tension and compression forces, the area of concrete in compression can be solved for, as all other parameters are known. However, unlike structures with constant cross-sections, here the compression depth a is determined by analyzing the TPMS cross section at midspan, imposing the area to the top of the cross-section and abstracting the resulting a.

In accordance with ACI 318-19 code [11] a strength reduction factor of $\phi = 0.9$ is applied, assuming that

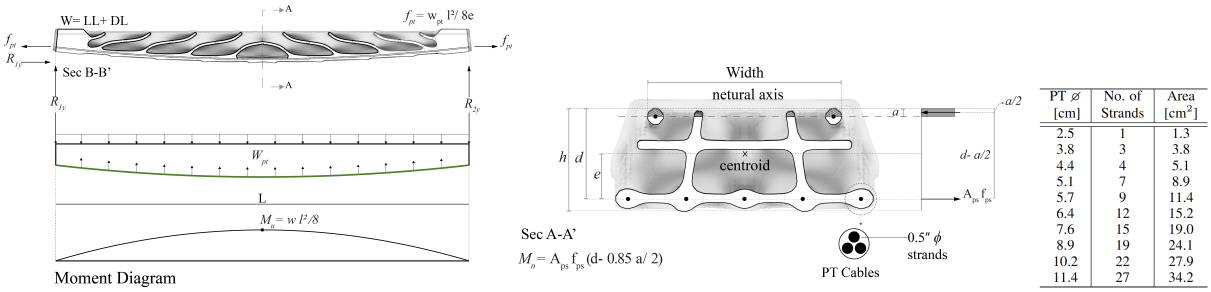

PT ⌀ [cm]	No. of Strands	Area [cm^2]
2.5	1	1.3
3.8	3	3.8
4.4	4	5.1
5.1	7	8.9
5.7	9	11.4
6.4	12	15.2
7.6	15	19.0
8.9	19	24.1
10.2	22	27.9
11.4	27	34.2

Figure 3: For a simply supported TPMS structure, the maximum applied bending moment, M_u, is determined based on the distributed load, w accounting for both live loads, LL applied along the whole top surfce and dead loads, DL (self-weight). Representative cross-section is shown at midspan of a TPMS structure with corresponding simplified stress block to calculate nominal moment capacity, M_n. The post-tensioning cable is assumed to be made from 1.27 cm diameter strands, and the respective amount of strands in a variety cable diameters ⌀are reported in the accompanying table [8, 9, 10].

the section is tension controlled. Future work will explore alternatives, compression-controlled sections, as the TPMS structure is post-tensioned in which the steel cable's yield strength is typically larger than standard rebar. Hence, the concrete in compression may reach its strain limit prior to the tension steel reaches or exceeds its tensile strain limit. However, here the intention is to propose an approximate analysis for large scale TPMS structures compared to incumbent spanning structures. Large scale testing of the 10-meter TPMS structure, DIAMANTI, indicated that the design was ductile, reflecting a tension-controlled section.

The prefabricated, modular TPMS structure is post-tensioned to not only unify the structure, as intended with the two top cables in the TPMS design, but to also enhance performance, serviceability and resiliency, as well as reducing the amount of concrete needed, resulting in a lighter and economical system. Additionally, post-tensioned concrete structures can limit deflections under loading, reducing the amount of bending, particularly beneficial for enabling long spans. To determine the appropriate post-tensioning jacking forces, the cables threaded throughout the spanning system are assumed to have parabolic profiles, drapes, corresponding to the external, funicular form of a cable under a uniformly distributed applied load. The parabolic profile enables for the cross-section to be placed in compression [4], resist bending moments, and control deflections.

To calculate the needed post-tensioning force to counteract both the applied live loading and self-weight of the structure, an equivalent distributed load generated by the cable is assumed (Fig. 3). The total post-tensioning force, f_{PT} is calculated as:

$$f_{PT} = \frac{w_{PT} l^2}{8e} \tag{2}$$

where w_{PT} is set equal to the applied uniform load that is being counteracted and e is the eccentricity, distance between the cable and the centroid of the cross-section at mid-span, of the cable (Fig. 3). Hence, the jacking force in the cable is determined based on the counteracting bending moment caused the curvature and eccentricity of the post-tensioned cable. For simplicity, this work assumed that the post-tension cables start at the centroids of the cross-sections at the ends of the TPMS structures and the determined post-tensioning force is equally distributed along the cables.

2.3. Design Objective, Variables, and Constraints

With the capability of generating TPMS structures at varying spans and assessing their flexural strength and required post-tensioning force, the following design object and constraints are considered:

$$\begin{aligned} &\text{Objective:} \quad \phi M_n \geq M_u \\ &\text{s.t.} \qquad\quad f_{PT} < 0.8 f_{py} \end{aligned}$$

where the reduced nominal moment capacity must greater than the maximum applied bending moment, M_u. Here, the bending moment accounts for both an applied distributed live load, LL applied uniformly across the top surface and the TPMS structures dead load, DL (self weight). The TPMS structure is assumed to be simply supported with a parabolic cable profile. A permissible tensile stress constraint is set whereby the force applied to the post-tension cable must not exceed 80% of the steel cables yield strength [8, 9]. To achieve the objective and satisfy the constraint, the amount of post-tensioning cables and strands within each are considered as design variables. Notably, if additional cables are added, the generated geometry is altered to accommodate additional conduits, slightly increasing the structure's self-weight and altering the cross-section.

To illustrate the design alteration process, Fig. 4 demonstrates how an initial structure, starting with two

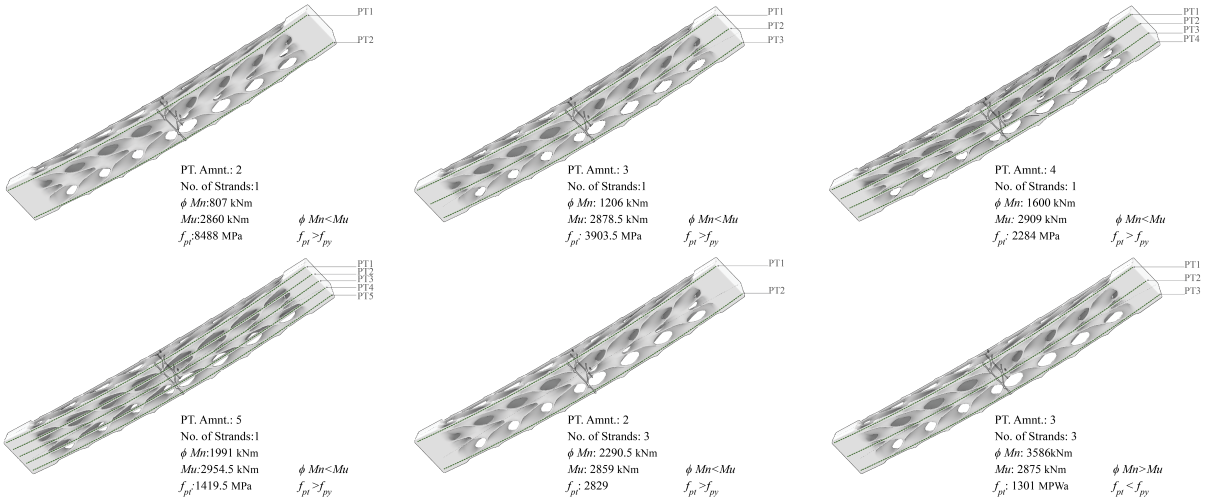

Figure 4: Illustrative example of the design alteration process, whereby post-tensioning cables and amount of strands are increased until both the design objectives and constraints are satisfied. All generated TPMS structures are initialized with two cables, each with a single strand (*top left*). An iterative alteration process is conducted until the design (*bottom right*) has a reduced nominal moment capacity greater than the applied bending moment, and all cables are not overstressed.

post-tensioning cables with the lowest amount of strands identified in Fig. 3 reference table, is iterated, altered five times. For the first iteration, an additional cable with a single strand is added along mid-span, yet both the objective and constraints are not satisfied. The process of adding cables is continued, placing cables at equal subdivisions along the bottom of the structure until five cables have been added, at which point the resolution of the TPMS geometry becomes too dense. Hence, instead of adding additional cables, the number of cables is reset to two and the amount of strands within each cable is incremented to the next largest value, for this example, three strands. Cables with three strands are again added until the structure satisfies both the objective and constraint.

3. Pedestrian Bridge Application

The iterative design process developed in Section 2 is applied here for a pedestrian bridge application. To show the flexibility of the approach, six TPMS structures are generated at different spans, 10, 20, and 30 meters, each considering a deck width of either 2 or 3 meters. Based on the PGS form-diagram, the depths at each span from least to greatest are 1, 1.5, and 2 meters, respectively. Each design considers the following characteristics and material properties: applied live loading of 4.3 kN/m^2 [12], concrete density of 2,200 kg/m^3, $f'_c = 20,684\ kN/m^2$, and $f_{py} = 1,861\ MPa$. All six generated designs, that satisfy the specified objective and constraints in Section 2.3 are shown in Fig. 5. The designs spanning 10 meters require the least amount of post-tensioning reinforcement. While the 30 meter span design also requires few cables, each cable requires three strands, resulting in a larger amount of post-tensioning reinforcement compared to both the 10 and 20 meter spanning structures. Additional details for all designs are reported in Table 1. Each mass is determined from an approximated 3D printed toolpath assuming a print width of 21 mm and 8 mm height.

To further evaluate the TPMS structures, all six designs are compared to incumbent standard, prismatic beams spanning the same distances and having the same applied live load uniformly distributed across

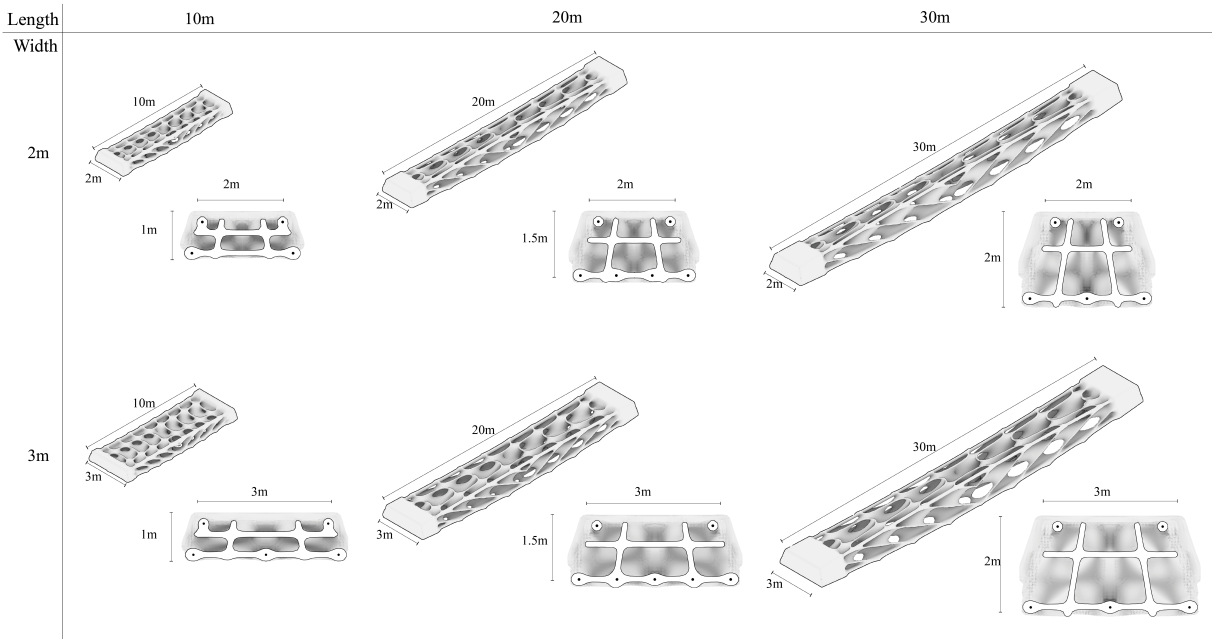

Figure 5: Generated pedestrian bridge concepts at varying spans, widths, and depths. Corresponding cross sections at mid-span for each design are shown along with the location and amount of post-tensioning cables, indicated by black solid circles.

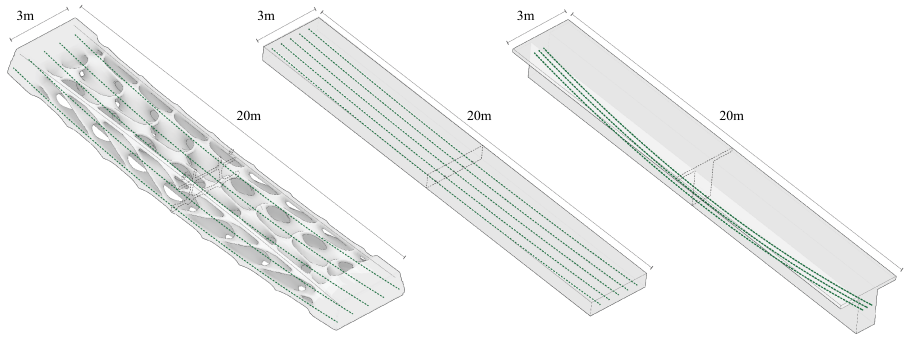

(a)

(b)

Figure 6: (a) 20 meter spanning proposed TPMS structure compared to rectangular and "T" cross section incumbent beams. (b) Images of the fabrication and construction of the 10 meter DIAMANTI structure, showcasing not only the feasibility of achieving large scales but also indicating how unlike conventional casted, solid concrete incumbents, TPMS structures are concrete 3D printed. Image courtesy of SIKA.

Table 1: Comparison of spanning structures with TPMS cross-sections (TPMS) to T-cross section (T-Sec.) and rectangular cross section (Rect. Sec.) prismatic beams. All designs have equivalent volumes and satisfy $\phi M_n \geq M_u$ as well as $f_{pt} \leq 0.8 f_{py}$. Percent difference of $kgCO_2e$ accounts for the change in total carbon dioxide emissions from both the cement and steel strand production. Overall the proposed TPMS structures reduce $kgCO_2e$ about 70% compared to the incumbents, attributed to needing less cement and steel reinforcement.

	Width [m]	Depth* [m]	PT. Amnt.	No. of Strands	f_{pt} [MPa]	M_u [kN-m]	ϕM_n [kN-m]	Concrete Mass [kg]	PT Reinf. Mass [kg]	% Diff. $kgCO_2e$
30-meter span										
TPMS	3	2.00	3	3	1,301	2,875	3,586	37,979	211	
T-Sec.	3	1.68	4	12	1,155	6,357	9,592	130,831	1,125	72
Rect. Sec.	3	0.66	5	27	1,330	6,357	8,489	130,831	3,164	77
TPMS	2	2.00	3	3	1,001	2,131	3,326	31,020	211	
T-Sec.	2	1.50	4	9	1,456	5,064	7,165	109,230	844	72
Rect. Sec.	2	0.83	5	15	1,468	5,064	8,354	109,230	1,758	75
20-meter span										
TPMS	3	1.50	5	1	953	1,239	1,316	23,751	78	
T-Sec.	3	1.48	3	7	1,222	2,605	4,205	78,409	328	70
Rect. Sec.	3	0.59	5	12	1,392	2,605	5,061	78,409	938	73
TPMS	2	1.50	4	1	1,052	893	1,052	18,513	63	
T-Sec.	2	1.24	3	7	1,172	1,965	4,192	61,381	328	71
Rect. Sec.	2	0.70	5	7	1,487	1,965	3,874	61,381	547	72
10-meter span										
TPMS	3	1.00	3	1	980	286	497	9,998	23	
T-Sec.	3	1.21	5	1	1,380	578	997	33,374	39	69
Rect. Sec.	3	0.51	4	4	1,413	578	1,366	33,374	125	71
TPMS	2	1.00	2	1	1,460	203	334	7,637	16	
T-Sec.	2	0.96	5	1	1,346	414	992	24,527	39	69
Rect. Sec.	2	0.56	5	3	1,195	414	1,155	24,527	117	70

* T-section depth denotes the section's total distance from top to bottom where the flange depth is constant at 0.15 meters for all designs. The reported T-section's width is the top distance and the T-stem's width is 1 meter for all.

equivalent top surface areas, as well as the same volumes. Specifically, one beam has a "T" cross-section and the other has a rectangular cross-section, as illustrated in Fig. 6(a).

All design characteristics and attributes of the six TPMS structures and their respective incumbents are reported in Table 1. Each design satisfies the flexural strength design objective and post-tensioning constraint. The TPMS structures require less post-tensioning cables with the least amount of strands in all cases. The mass for each incumbent is determined by multiplying the solid volume by the density of concrete, as if casted, whereas the TPMS structures' mass is calculated from the sliced geometry used for 3D printing. The difference in applied bending moment M_u, is attributed to the difference in self-weight. For example, all structures spanning 30 meters with a 3 meter top deck width have an applied $\approx$13 kN/m live load; however, each have their own dead load determined from their respective 3D-printed or casted concrete self-weight.

To assess environmental impacts associated with the differences in the concrete mass and amount of the post-tensioning reinforcement, the designs are assessed by the amount of carbon dioxide emitted in the production of cement and steel required. Based on the U.S. national average, approximately 0.173 $kgCO_2e$/kg of concrete [13] and 2.75 $kgCO_2e$/kg of steel [14] is emitted. These multipliers are applied to determine the percent difference in equivalent carbon dioxide emission for each design alternative. Overall, the TPMS structures reduce carbon dioxide emissions by about 70%.

Figure 7: Future use case of large scale concrete 3D-printed, post-tensioned TPMS structures as architectural and engineering design solutions. Rendering courtesy of Massive Form.

4. Closing Remarks

This works develops upon the paradigm shift inspired by DIAMANTI in the architectural and structural engineering design process, where material performance, natural and complex geometric forms, and digital fabrication converge to challenge long-standing conventions in construction. Through the integration of periodic anticlastic surfaces, specifically diamond triply periodic minimal surface geometries, post-tensioned assembly, as well as sustainable and economical construction strategies, this work demonstrates the potential of computational design to drive innovation in efficiency, economy, and elegance (Fig. 7). By embedding force-informed geometries directly into the structural logic of 3D-printed concrete elements, the TPMS design alternatives articulate a new structural language rooted in the efficient use of material, resiliency, and the expressive potential of digitally enabled fabrication. As the architectural and structural engineering fields continue to seek solutions to pressing environmental demands, DIAMANTI serves not merely as a concept, but as a strategic approach seeking a future where sustainability and performance are inherently interconnected.

Future work will consider how 3D printing constraints affect flexural strength by altering the geometry, concrete cross-section, such that overhangs are reduced. Additional considerations for material properties will be considered to account for concrete strength and carbonation potential since more sustainable materials are constantly emerging and applicable at scale. The inclusion of these materials, as long as they satisfy the set objectives and constraints, will further benefit from the enhanced surface area offered by the TPMS structures.

Acknowledgments

The authors acknowledge the support provided by the Advanced Research Projects Agency Energy (ARPA-E) Grant - U.S. Department of Energy (DE-AR0001631). This research was partially funded by the National Science Foundation CAREER Award (NSF CAREER-1944691 CMMI) awarded to Masoud Akbarzadeh.

References

[1] M. Akbarzadeh, H. Chai, Y. Zhi, M. E. Ororbia, T. Teng, M. Bernhard, D. Bolhassani, F. Yavartanoo, J. Tapia, K. Pajak, M. Bernard, L. Trousset, P. Kassabian, and B. Waligun, "Diamanti: 3d-printed, post-tensioned concrete canopy," *FABRICATE: Creating Resourceful Futures*, pp. 292–301, 2024.

[2] Parametric Architecture. "Diamanti canopy debuts in venice with sustainable 3d-printing." (2025), [Online]. Available: https://parametric-architecture.com/diamanti-canopy-debuts-in-venice-with-sustainable-3d-printing/.

[3] M. Ororbia, H. Chai, Y. Zhi, P. Vakhshouri, J. Chacon, J. Yost, M. Bernhard, F. Yavartanoo, J. Tapia, D. Bolhassani, M. Bernard, L. Trousset, K. Pajak, B. Waligun, P. Kassabian, and M. Akbarzadeh, "Experimental study of a funicular concrete beam prototype," in *Proceedings of IASS Annual Symposia*, International Association for Shell and Spatial Structures (IASS), vol. 2024, 2024.

[4] H. Chai, M. E. Ororbia, Y. Zhi, R. Welch, B. Faircloth, F. Yavartanooc, D. (Bolhassani, and M. Akbarzadeh, "Design approach for a post-tensioned funicular concrete beam," in *Proceedings of the IASS 2024 Symposium: Redefining the Art of Structural Design*, P. Block, G. Boller, C. DeWolf, J. Pauli, and W. Kaufmann, Eds., Zurich, Switzerland, Aug. 2024.

[5] H. Chai, Y. Lu, M. Hablicsek, and M. Akbarzadeh, "Generation of a compression-tension combined funicular polyhedral beam structure," in *Proceedings of IASS Annual Symposia*, International Association for Shell and Spatial Structures (IASS), 2023, pp. 1–11.

[6] M. Akbarzadeh, *Polyhedral Graphical Statics: For Funicular Structural Form Finding*. London: Cambridge University Press, 2025.

[7] M. Akbarzadeh, "3d graphic statics using polyhedral reciprocal diagrams," Ph.D. dissertation, ETH Zürich, Zürich, Switzerland, 2016.

[8] Post-Tensioning Institute, *Post-Tensioning Manual*, 3rd. Phoenix, AZ: Post-Tensioning Institute, 1985.

[9] K. D. Bondy and B. Allred, *Post-Tensioned Concrete: Principles and Practice*. Lulu. com, 2017.

[10] AMSYSCO, Inc. "Material properties of post-tension strands." (Jan. 2010), [Online]. Available: https://www.amsyscoinc.com/2010/01/29/material-properties-of-post-tension-strands/.

[11] American Concrete Institute, *Building Code Requirements for Structural Concrete (ACI 318-19) and Commentary*. Farmington Hills, MI: American Concrete Institute, 2019, ACI 318-19, ISBN: 9780870313624.

[12] AASHTO, *AASHTO LRFD bridge design specifications*. Washington, D.C.: American Association of State Highway and Transportation Officials, 2008.

[13] National Ready Mixed Concrete Association, "Environmental product declaration: Nrmca member industry-wide epd for ready mixed concrete," NSF International, Silver Spring, MD / Ann Arbor, MI, Type III environmental product declaration EPD 10080, Oct. 2016.

[14] KT Innovations (KieranTimberlake) / Building Transparency. "Tally® – lca, life-cycle environmental impact analysis app for autodesk revit." (2025), [Online]. Available: http://choosetally.com/.